ADVANCED ENERGY MATERIALS
www.advenergymat.de

Nominal Lanthanum Niobate, a Versatile Additive for Reducing Grain Boundary Resistance in Conductive Ceramics

Limin Liu, Yujian Liu, Xiaoliang Zhou, Frank Tietz, Daniel Grüner, Tingting Yang, Lei Jin,* Xingyu Liu, Jürgen Malzbender, Ruth Schwaiger, Rafal E. Dunin-Borkowski, and Qianli Ma**

Conductive ceramics currently play a vital role in human life. In practical applications, most conductive ceramics are polycrystalline, and their overall conductivity (σ_{total}) is influenced by both bulk and grain boundary resistances (R_{bulk} and R_{gb}, respectively). While R_{bulk} is mainly of academic interest, R_{gb} often determines the quality of a conductive ceramic component. Currently, studies discussing the influence of specific methods on grain boundary resistances are typically related to individual ceramics. In this study, it is discovered that the addition of 0.5–3 mol% nominal $LaNbO_4$ significantly reduces the R_{gb} of several well-known conductive ceramics, such as rhombohedral NaSICON-type Na^+-ion-conducting $Na_{3.4}Zr_2Si_{2.4}P_{0.6}O_{12}$ and Li^+-ion conducting $Li_{1.5}Al_{0.5}Ti_{1.5}P_3O_{12}$, Li^+-ion-conducting tetragonal perovskite $Li_{0.34}La_{0.56}TiO_3$, oxygen-ion-conducting cubic fluorite 8 mol% Y_2O_3 stabilized ZrO_2, and electron-conducting perovskite $SrTiO_3$ (sintered in a reducing atmosphere). In particular, for NZSP and LATP, the enhanced σ_{total} reaches 9.3×10^{-3} S cm^{-1} and 2.1×10^{-3} S cm^{-1} at 25 °C, surpassing previously published results. Detailed investigations reveal that the microstructure of the grain boundaries in all the ceramics undergoes significant improvements. The findings elevate the importance of research on grain boundaries, inspiring the development of conductive ceramics with higher σ_{total} for superior applications.

1. Introduction

Conductive ceramics currently play a vital role in human life due to their wide range of applications, for example in electronic components, sensors, catalysis, energy conversion, or storage systems. Here, the ceramics are defined as non-metallic inorganic materials which are crystallized, strengthened, and densified by heat treatment (sintering). Most of the applied conductive ceramics are polycrystalline materials due to their cost-effectiveness compared to single-crystalline materials. The overall resistance, R_{total}, of conductive polycrystalline ceramics is usually composed of two contributions: the grain interior or bulk resistance, R_{bulk}, and the transgranular grain boundary resistance, R_{gb}. While materials scientists predominantly focus on R_{bulk} as an intrinsic property of the ceramic that is strongly related to the transport mechanism in the individual material, R_{gb} is often regarded as an unavoidable fact due to the existence of inadequate grain-to-grain contact and secondary phases along the grain boundaries, which can consist of crystalline and amorphous phases. Although R_{gb} may contribute negligibly to R_{total} in some cases, such as properly prepared Y_2O_3-stabilized ZrO_2 (YSZ, cubic phase),[1] it can also contribute equally as R_{bulk} or become the dominant contribution of R_{total}. In ceramics with a lower crystal symmetry than cubic structure, high R_{gb} can be induced by thermal expansion anisotropy, which is defined as the difference between the thermal

L. Liu, Y. Liu, X. Zhou
School of Chemistry and Chemical Engineering
Southwest Petroleum University
Chengdu 610500, P. R. China
E-mail: xlzhou_swpu@sina.com

The ORCID identification number(s) for the author(s) of this article can be found under https://doi.org/10.1002/aenm.202404985

DOI: 10.1002/aenm.202404985

L. Liu, X. Zhou
Tianfu Yongxing Laboratory
Chengdu 610213, P. R. China

F. Tietz, D. Grüner, X. Liu, J. Malzbender, R. Schwaiger, Q. Ma
Institute of Energy Materials and Devices (IMD)
Forschungszentrum Jülich GmbH
52425 Jülich, Germany
E-mail: q.ma@fz-juelich.de

T. Yang, L. Jin, R. E. Dunin-Borkowski
Ernst Ruska-Centre for Microscopy and Spectroscopy with Electrons
Forschungszentrum Jülich GmbH
52425 Jülich, Germany
E-mail: l.jin@fz-juelich.de

Table 1. Fundamental information concerning the pristine and $LaNbO_4$-modified samples.

Sample name	$LaNbO_4$ amount for modification [mol%]	Powder preparation method	Theoretical density [g cm^{-3}]	Sintering temperature for pristine and modified samples [°C]	Relative density of pristine sample [%]	Relative density of modified sample [%]
NZSP	2	SASSR	3.3	1260	96	97
LATP	3	SASSR	2.9	950	95	96
LLT	2	Pechini + SSR	5.0	1325	96	97
8YSZ	0.5	Pechini	6.0	1400	97	94
$SrTiO_3$	1	Pechini	5.1	1400	93	93

expansion coefficients (TECs) of different lattice parameters. Prime examples are the NaSICON-type $Na_{3.4}Zr_2Si_{2.4}P_{0.6}O_{12}$ (NZSP) and $Li_{1.5}Al_{0.5}Ti_{1.5}P_3O_{12}$ (LATP),[2,3] classical solid-state sodium and lithium-ion conductors, respectively, both crystallizing with rhombohedral symmetry. Their TEC along the rhombohedral *a* axis is much lower than that of the *c* axis, leading to contact degradation between the grains due to anisotropic contraction after the sintering process and resulting in a significant increase in R_{gb}. The difference between R_{gb} and R_{bulk} in these materials can be as high as one order of magnitude.[2–5] Since this thermal expansion behavior is an intrinsic property of the materials, the elimination of such differences is extremely challenging.

R_{gb} may also be determined by microstructural features such as the grain size distribution. As an example, in YSZ, R_{gb} can also dominate R_{total} when the sintered grains of YSZ are nanocrystalline, since the volumetric ratio of grain boundaries to grains is then much higher than in YSZ with grains of several micrometers.[6]

In many cases, the reasons for high R_{gb} in ceramics are not clear due to the complexity of grain boundary formation and the difficulties in its characterization. For instance, the R_{gb} of $Li_{3x}La_{0.67-x}TiO_3$ is orders of magnitude higher than R_{bulk}, but the exact reasons for this have been debated for decades. $Li_{3x}La_{0.67-x}TiO_3$ has a pseudo-cubic perovskite structure with a tetragonal phase. Unlike NaSICON-type NZSP and LATP, it has a weak thermal expansion anisotropy effect because of the higher crystal symmetry. The explanations for its high R_{gb} vary. They range from the significant depletion of lithium ions in the grain boundaries – which leads to layers with thicknesses of several unit cells composed of a binary Ti–O compound, obstructing the accommodation and transport of the charge carrier, and resulting in a lower grain boundary conductivity[7]—to the formation of space charge layers in the grain boundaries[8] and numerous domain boundaries in a single $Li_{3x}La_{0.67-x}TiO_3$ grain, which may have a more pronounced contribution to R_{gb} compared to grain boundaries.[9] Specific methods have been employed to decrease R_{gb} in certain ceramics, such as modifying the microstructure of the grains,[1–3,6] altering the chemical environment of the grain boundaries,[10–13] narrowing the space charge layer in grain boundaries,[14,15] rectifying the misorientation of grain boundaries,[16] or even activating grain boundaries through optical illumination.[17] However, these studies have been limited to specific methods that affect grain boundary resistances in individual ceramics. No universal method that is suitable for multiple ceramics has been reported so far.

Monoclinic lanthanum niobate ($LaNbO_4$) is a ferroelastic material that contains domains in two crystallographic orientations separated by highly mobile boundaries, exhibiting rubber-like behavior and a shape-memory effect.[18–20] Several previous reports have demonstrated its effectiveness in improving the mechanical properties when present in the grain boundaries of ceramics such as Al_2O_3, YSZ, and CeO_2-stabilized zirconia.[21–25] Since such modifications of grain boundaries can enhance the mechanical properties of ceramics, it is reasonable to assume that they may also be effective in reducing R_{gb} due to the improved grain-to-grain contact. However, this assumption has yet to be verified.

In this study, we added 0.5–3 mol% $LaNbO_4$ into various well-known conductive ceramics, namely NZSP and LATP with a rhombohedral structure, $Li_{0.34}La_{0.56}TiO_3$ (LLT), $Y_{0.148}Zr_{0.852}O_{2-\delta}$ (8YSZ), and $SrTiO_3$ with (pseudo-)cubic structures. In all these ceramics, a significantly reduced R_{gb} was observed. For NZSP and LATP in particular, the σ_{total} was significantly enhanced, reaching 9.3×10^{-3} S cm^{-1} and 2.1×10^{-3} S cm^{-1} at 25 °C, respectively, surpassing previously published results. Detailed investigations using scanning electron microscopy (SEM) and scanning transmission electron microscopy (STEM) revealed that the microstructure of the grain boundaries in all the ceramics underwent significant improvements in terms of better grain-to-grain contact, fewer micro-cracks, a narrower width, and a higher density of the grain boundary region. As a result, we successfully discovered an effective inhibitor for R_{gb} across a wide range of ceramics.

2. Results and Discussion

2.1. Conductivities

The NZSP, LATP, LLT, 8YSZ, and $SrTiO_3$ samples were modified with 0.5-3 mol% $LaNbO_4$ (**Table 1**). The amount of $LaNbO_4$ added to all the compositions was previously optimized. The compositions for the optimization are shown in Table S1 (Supporting Information). The pristine and modified NZSP and LATP powders were prepared by a solution-assisted solid-state reaction method (SASSR).[26] The pristine LLT powder was prepared by Pechini's method,[27] which is regarded as a sol–gel method. The modified LLT powder was prepared by solid-state reaction, mixing the proper amounts of La_2O_3 and Nb_2O_5 with pristine LLT powder by means of ball milling. The pristine and modified 8YSZ and $SrTiO_3$ powders were also prepared by Pechini's method. The $SrTiO_3$ samples were sintered in a reducing atmosphere. The various preparation methods were applied to verify an influence of the synthesis method on the impact of the $LaNbO_4$ addition, but the grain boundary resistance clearly does not

depend on the preparation method. All pristine and modified samples of each material were exposed to the same sintering temperature and resulted in similar relative densities (Table 1), indicating that $LaNbO_4$ is not a sintering aid for the targeted ceramics. All samples show high relative densities between 93% and 97%, which is suitable for conductivity analysis. Because of the low $LaNbO_4$ content, all pristine and modified samples are highly pure materials, with a very small amount or even non-observable secondary phases in the X-ray diffraction (XRD) patterns. There are also unnoticeable phase differences observed between pristine and modified samples (Figure S1, Supporting Information).

The impedance spectrum and the Arrhenius plot of pristine NZSP are taken from a previous publication.[2] All other data are collected experimentally in the present study. The σ_{total} and σ_{bulk} of the pristine and modified samples are determined by fitting Nyquist plots of the impedance spectra. To facilitate comparisons between the different samples, the impedance spectra are normalized with the sample geometries. The equivalent circuit for fitting the impedance spectra is shown in **Figure 1a**, where *L*, *R*, and CPE indicate the inductance, resistance, and constant phase element (CPE), respectively. The key parameters of an equivalent circuit in Figure 1a are shown in Table S2 (Supporting Information). For NZSP and LATP samples, it is common that only one (or even half) of the semi-circles appears in the impedance spectrum at room temperature (RT) due to the limited frequency range (up to 10 MHz) of conventional impedance spectroscopy systems. It is therefore challenging to precisely distinguish between the contributions of R_{bulk} and R_{gb}. In this study, two impedance spectroscopy systems were combined to overcome this issue, covering high frequency (HF) and normal frequency (NF) ranges from 3 GHz to 1 MHz and from 10 MHz to 0.01 Hz, respectively. As shown in Figure 1a, both the pristine and modified NZSP and LATP exhibit nearly two complete semi-circles, facilitating the differentiation of R_{bulk} and R_{gb}. This can also be determined just by NF impedance spectroscopy at low temperatures, since the time constant (τ) of the parallel RC element (R1 and CPE1) shifts towards the NF range because of the increased resistance of the samples at low temperatures. For LLT, YSZ and $SrTiO_3$, the NF range is sufficient to exhibit both semi-circles in the investigated temperature range (partially enlarged impedance spectra for $SrTiO_3$ are shown in Figure S2 (Supporting Information), where the first semi-circle could be observed). L0 is only applied for NZSP and LATP, since only these materials show an apparent inductance behavior in the impedance spectra. For all samples, the capacitances of CPE1, CPE2, and CPE0 align well with the characteristic capacitance originating from the bulk contribution (represented by R1 and CPE1), the grain boundary contribution (represented by R2 and CPE2), and the interface between ceramics and electrodes (represented by CPE0),[28] respectively (Table S2, Supporting Information). The only exception is the capacitances of CPE1 of $SrTiO_3$, which is discussed in the supporting information (Table S2, Supporting Information). Consequently, for all the samples, R1 and R2 are attributed to R_{bulk} and R_{gb}, respectively, while R_{total} equates to $R_{bulk} + R_{gb}$. Evidently, the σ_{bulk} values of all the pristine and modified samples are very similar, with the notable difference in their σ_{total} primarily arising from the grain boundary contribution.

All σ_{bulk} and σ_{total} values exhibit linear behavior in the Arrhenius plot (Figure 1b), except for $SrTiO_3$. The non-linear Arrhenius behavior observed in reduced $SrTiO_3$ is not surprising.[29] The reduction of Ti^{4+} to Ti^{3+} creates electrons in the 3d conduction band, resulting in semiconducting or even metal-like behavior depending on the electron concentration.[30] However, reduced $SrTiO_3$ is inherently unstable in the presence of air, as Ti^{3+} gradually oxidizes back to Ti^{4+}. This oxidation process is accelerated at higher temperatures, leading to the non-linear behavior observed in the Arrhenius plot. For all other samples, the activation energy (E_a) of σ_{bulk} for both the pristine and modified samples are similar to each other, while the E_a of σ_{total} of the modified samples is noticeably lower than that of the pristine samples. This is attributed to their lower R_{gb} compared to the pristine samples. All the conductivities and activation energies (E_a) obtained from Figure 1a,b, respectively, are shown in **Table 2**.

The significant difference between the σ_{bulk} and the σ_{total} of the pristine NZSP can be attributed to consequences of the thermal expansion anisotropy, causing the contact degradation between the grains after the sintering process and resulting in a higher R_{gb}.[2] The σ_{total} of the pristine NZSP in this study was already optimized by the preparation method and grain control, making it the material with one of the highest reported conductivity values (5.2×10^{-3} S cm^{-1} at RT) among all polycrystalline NaSICON-type materials, comparable to the state-of-the-art Na^+-ion-conducting liquid electrolyte of 1 M $NaClO_4$ in the mixture of ethylene carbonate and dimethyl carbonate.[2,5,31] The R_{gb} of $LaNbO_4$-modified NZSP is further decreased. The resulting σ_{total} (9.3×10^{-3} S cm^{-1} at RT) of the modified NZSP surpasses previously published results of Na-ion-conducting polycrystalline oxides. Higher Na^+-ion conductivity at RT is only reported for single crystalline β''-alumina (1.3×10^{-1} S cm^{-1}),[32] polycrystalline $Na_2(CB_9H_{10})(CB_{11}H_{12})$ (7.0×10^{-2} S cm^{-1}),[33] and polycrystalline $Na_{2.88}Sb_{0.88}W_{0.12}S_4$ (3.2×10^{-2} S cm^{-1}).[34] A detailed comparison is shown in Figure S3 (Supporting Information). For verification of the beneficial influence of nominal $LaNbO_4$ on R_{gb} in polycrystalline NZSP, La and Nb sources are separately added to pristine NZSP. While the La-modified NZSP also exhibits a higher σ_{total} compared to pristine NZSP (6.7×10^{-3} S cm^{-1} vs 5.2×10^{-3} S cm^{-1}, respectively, Figure S4, Supporting Information), the increase is still much lower than that observed in $LaNbO_4$-modified NZSP (9.3×10^{-3} S cm^{-1}). Instead, Nb-modified NZSP shows a σ_{total} of 5.3×10^{-3} S cm^{-1} at RT, which is nearly the same as that of the pristine sample (Figure S4, Supporting Information). This suggests that the superior σ_{total} of $LaNbO_4$-modified NZSP arises from the combined influence of both La and Nb, rather than the impact of the single. Previous publications have also discussed La and Nb substitution in NaSICON ceramics,[31,35] assuming that La or Nb cations occupy Zr positions. In these reports, the σ_{total} increased up to 3.4×10^{-3} and 5.5×10^{-3} S cm^{-1} at RT for La and Nb substitutions, respectively. The values are far below those observed in the present study, in which nominal $LaNbO_4$ is only considered as a mixture in the polycrystalline NZSP.

The σ_{total} of the pristine LATP in this study (9.5×10^{-4} S cm^{-1}) is also among the highest values reported so far.[36] The σ_{total} of the modified LATP (2.1×10^{-3} S cm^{-1}), while not as high as the complex sulfide $Li_{9.54}Si_{1.74}P_{1.44}S_{11.7}Cl_{0.3}$

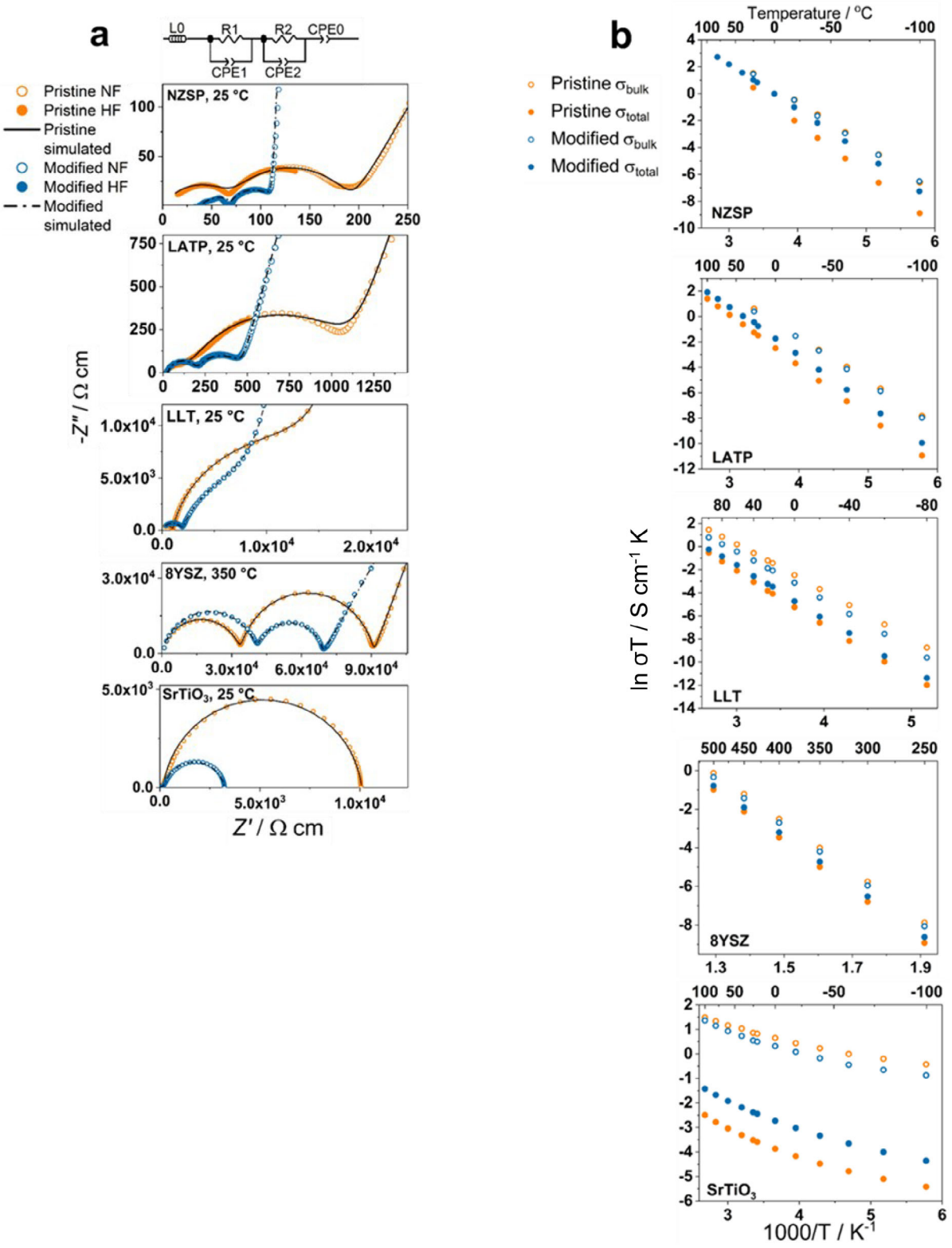

Figure 1. a) Impedance spectra with gold electrodes using a high-frequency (HF) and a normal-frequency (NF) analyzer, together with the fitted data for both pristine and $LaNbO_4$ modified NZSP, LATP, LLT, 8YSZ (Ag electrodes are applied) and $SrTiO_3$. The spectra are corrected for dimensional variations. b) Arrhenius plot of σ_{total} and σ_{bulk} of the samples in (a).

Table 2. Conductivities obtained from Figure 1a and E_a derived from Figure 1b.

Sample name		σ_{bulk} [S cm^{-1}]	σ_{total} [S cm^{-1}]	E_a of σ_{bulk} [eV]	E_a of σ_{total} [eV]
NZSP	Pristine	1.5×10^{-2}	5.2×10^{-3}	0.28	0.32
	Modified	1.4×10^{-2}	9.3×10^{-3}	0.28	0.29
LATP	Pristine	6.0×10^{-3}	9.5×10^{-4}	0.29	0.34
	Modified	5.0×10^{-3}	2.1×10^{-3}	0.30	0.32
LLT	Pristine	1.0×10^{-3}	7.2×10^{-5}	0.35	0.40
	Modified	5.1×10^{-4}	1.3×10^{-4}	0.36	0.39
8YSZ	Pristine	3.0×10^{-5}	1.1×10^{-5}	1.08	1.10
	Modified	2.4×10^{-5}	1.4×10^{-5}	1.07	1.08
$SrTiO_3$	Pristine	7.9×10^{-3}	9.9×10^{-5}	–	–
	Modified	5.8×10^{-3}	3.1×10^{-4}	–	–

(2.5×10^{-2} S cm^{-1}),[37] surpasses previously published results of Li^+-ion-conducting polycrystalline oxides, including the materials based on state-of-the-art $Li_7La_3Zr_2O_{12}$ (LLZO).[38,39] Details are provided in Figure S3 (Supporting Information). Similar to NZSP ceramics, La and Nb sources are added separately to pristine LATP to ascertain the influence of nominal $LaNbO_4$. While La or Nb-modified LATP also exhibits higher σ_{total} compared to pristine LATP (1.3×10^{-3} or 1.5×10^{-3} S cm^{-1}, respectively, Figure S5, Supporting Information), the increase is again much lower than that observed in $LaNbO_4$-modified LATP, indicating the combined influence of La and Nb on pristine LATP.

The σ_{bulk} values of modified LLT appear to be lower than those of the pristine compound, indicating that the addition of $LaNbO_4$ may enter the structure of LLT and influence the σ_{bulk}. In contrast, the σ_{total} of the modified LLT is noticeably higher than that of the pristine LLT, indicating a large difference of R_{gb} between pristine and modified LLT. The achieved σ_{bulk} and σ_{total} values of the pristine LLT are in good agreement with previous results.[40] The enhanced σ_{total} of modified LLT is among the best published results.[41]

The measured σ_{bulk} values of the pristine 8YSZ are also in good agreement with previous results.[1] The σ_{total} of 8YSZ may differ significantly according to the various grain sizes, preparation methods, and the presence of secondary phases,[1,6,13,42] which can either be negligible or several times lower than σ_{bulk}. Nevertheless, as the pristine and modified 8YSZ are prepared in the same way and possess similar microstructures in this study, the decrease of σ_{bulk} and the increase of σ_{total} for the modified 8YSZ at all tested temperatures indicate the effective reduction of R_{gb}.

Since $SrTiO_3$ is sintered in a reducing atmosphere, it is a semi-conductor with electrons as the major charge carriers. In combination with Au as electronic conductor and non-blocking electrode, the interface resistance between Au and $SrTiO_3$ is negligible.[43] The conductivity of $SrTiO_3$ differs strongly depending on the amount of oxygen vacancies, A or B-site deficiency, and element doping.[29,43–45] In the present study, the conductivities of both pristine and modified $SrTiO_3$ fall within a reasonable range. The significant difference in R_{gb} between the pristine and modified $SrTiO_3$ samples again highlights the effectiveness of grain boundary modification with $LaNbO_4$.

2.2. Microstructures and Their Influences

2.2.1. Microstructures of NZSP and LATP

The influence of thermal expansion anisotropy is evident in the microstructural SEM images of the pristine NZSP and LATP shown in **Figure 2**a,c, respectively. In both samples, many microcracks are visible, often originating from remaining small pores at triple grain junctions. It should be mentioned that the sample preparation of NZSP and LATP was carried out with Ar etching, which already minimizes the mechanical impact on the microstructures of the samples. When alternative methods are used involving mechanical forces, the loss of contact at the grain boundaries is significantly increased compared to the observations shown in Figure 2 (see Figure S6, Supporting Information).

For two adjacent grains of NZSP or LATP, when their lattice orientations are parallel with each other, the grain-to-grain contact is maintained during the cooling process of ceramic sintering, as the shrinkages of the grains in the direction of their interface and the direction perpendicular to their interface are equal. In general, the neighboring grains are misaligned with each other (e.g., $c \parallel a$), leading to a loss of contact between the grains, since one grain shrinks more in the direction of their interface while the other shrinks more in the direction perpendicular to their interface. This phenomenon is responsible for the insufficient grain-to-grain contact and the formation of microcracks along the grain boundaries (Figure 2a,c).

After the modification with $LaNbO_4$, the crack formation at the grain boundaries in both NZSP and LATP is significantly reduced (Figure 2b,d). For LATP in particular, the micro-cracks are almost fully eliminated, resulting in a superior increase of σ_{total} (2.2 times higher than that of the pristine LATP, Table 2). It is noteworthy that in both cases of NZSP and LATP, the pristine and modified samples exhibit similar grain sizes. This observation verifies that $LaNbO_4$ is not acting as a sintering aid for the samples, especially considering that the samples also possess similar sintering temperatures and relative densities (Table 1). Typically, a similar grain size results in a similar volume fraction of the grain boundaries within the ceramic, leading to similar R_{gb} contributions. However, the modified NZSP and LATP demonstrate decreased R_{gb} values with similar grain size like the pristine specimen, confirming the effectiveness of $LaNbO_4$ in reinforcing the grain contacts. In addition, in both modified

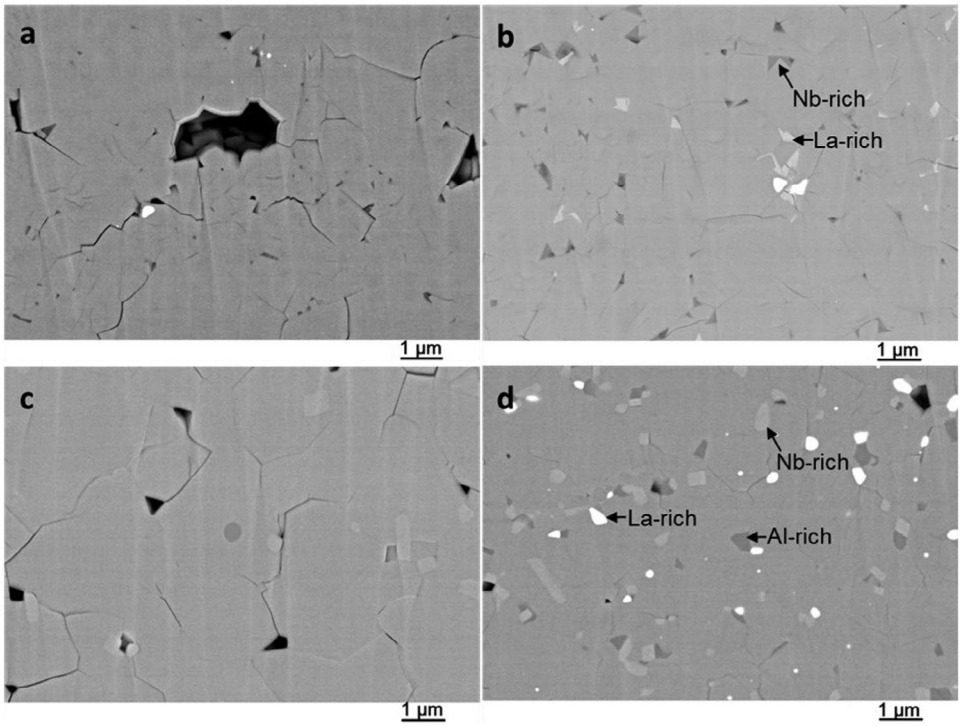

Figure 2. Backscattered electron SEM images of a) pristine NZSP, b) modified NZSP, c) pristine LATP, and d) modified LATP.

samples of NZSP and LATP, more secondary phases are formed. It seems that the remaining pores that are present in the pristine samples are filled by these secondary phases in the modified samples (Figure 2b,d). This is reasonable when La and Nb are not incorporated into the grains and are segregated at the grain boundaries and grain triple junctions. To demonstrate the secondary phases more clearly, STEM analysis with energy dispersive X-ray spectroscopy (EDS) was used (**Figure 3**). Since NZSP and LATP are sensitive to beam irradiation, which causes morphological changes and decomposition,[46] only limited magnification can be applied and atomic resolution is not possible in the present experimental setup. In the modified NZSP, a Nb-rich secondary phase is observed, which contributes primarily to the pore filling and, more remarkably, it can diffuse into the grain boundaries (Figure 3a), thus improving the grain-to-grain contact. However, it has been known that Nb_2-modified NZSP has no apparent improvement in σ_{total} (Figure S4, Supporting Information), indicating that La must also contribute to the reinforcement of the grain boundary of NZSP. In modified LATP, the triple junction pores are eliminated by three types of secondary phases, which are La-rich, Ti/Nb-rich, and Al-rich. No grain boundary diffusion/enrichment can be detected within the instrumental limit (Figures 2d and 3b).

2.2.2. Mechanical Properties of NZSP and LATP

To further confirm the grain boundary reinforcement observed in the SEM and TEM investigations, the mechanical properties of pristine and modified NZSP and LATP samples were analyzed, as presented in **Table 3**. The average elastic modulus (E_m) and fracture stress (Σ_f) were selected as representative parameters for the mechanical characteristics of the samples. These values were derived from the load-displacement curves obtained through ring-on-ring bending tests (a typical curve is shown in Figure S7, Supporting Information), following the guidelines outlined in the American Society for Testing and Materials (ASTM) C1499-05 standard.[47] E_m was calculated from the linear portion of the load–displacement curve, as unevenness in the specimen can cause non-linearity at low loads:

$$E_m = \frac{3\left(1-\nu^2\right)\cdot r_1^2\cdot \Delta F}{2\pi\cdot \Delta f\cdot t^3}\cdot \left[\left(\frac{r_2}{r1}\right)^2 - 1 - \ln\left(\frac{r_2}{r_1}\right) + \frac{1}{2}\left(\frac{1-\nu}{1+\nu}\right)\cdot\left(\frac{r_2^2-r_1^2}{r_3^2}\right)\cdot\left(\frac{r_2}{r_1}\right)^2\right] \quad (1)$$

where ΔF is the force difference and Δf the corresponding displacement change of the linear part, ν is the Poisson's ratio, t is the specimens' thickness, r_1, r_2 and r_3 are the radii of loading ring, supporting ring and specimen, respectively.

Σ_f is constant within the tensile loaded surface inscribed by the loading ring, i.e.:

$$\Sigma_f = \frac{3\left(1+\nu\right)\cdot F_f}{2\pi\cdot t^2}\left[\ln\frac{r_2}{r_1} + \left(\frac{1-\nu}{1+\nu}\right)\cdot\left(\frac{r_2^2-r_1^2}{2r_3^2}\right)\right] \quad (2)$$

where F_f is the fracture load. Other parameters are the same as in Equation 1.

Apparently, both E_m and Σ_f show an increase in the modified NZSP and LATP samples compared to their pristine

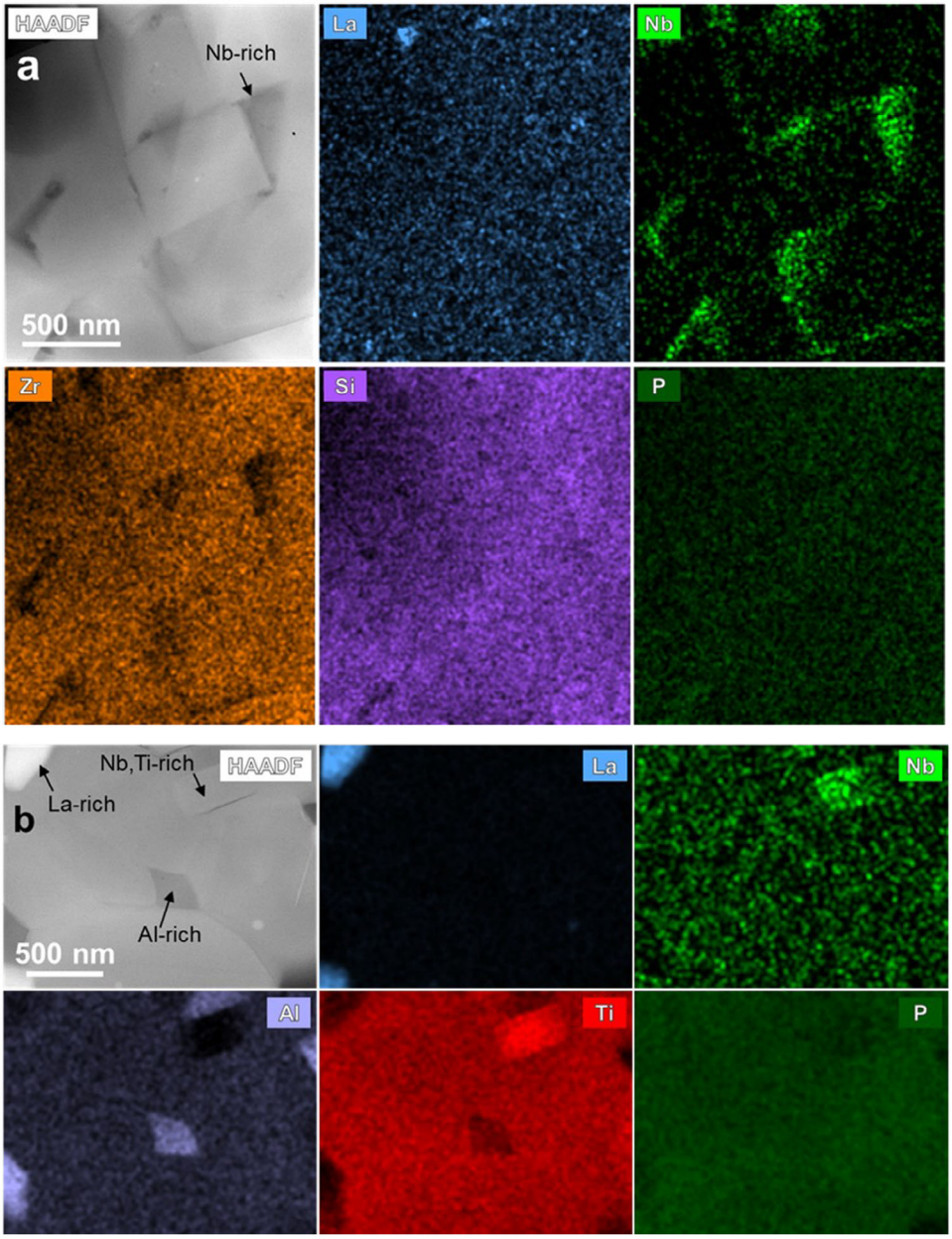

Figure 3. High-angle annular dark-field STEM images and background-subtracted EDS elemental maps of modified a) NZSP and b) LATP.

counterparts. The difference is particularly pronounced in LATP. Considering the microstructural differences between the pristine and modified samples (Figure 2), the improved reinforcement of grains and the reduced presence of microcracks in the modified NZSP and LATP are likely key factors contributing to the enhanced mechanical properties observed with the addition of nominal $LaNbO_4$.

2.2.3. Microstructures of LLT, 8YSZ, and $SrTiO_3$

Unlike NZSP and LATP, LLT, 8YSZ, and $SrTiO_3$ possess (pseudo-) cubic structures and exhibit no (or a weak) thermal expansion anisotropy effect. Micro-cracks are not observed in the pristine samples of LLT, 8YSZ, and $SrTiO_3$ (SEM images in Figure S8, Supporting Information), which means that they are not the main origin of the conductivity enhancement. Similar to the situation of NZSP and LATP, all pristine and modified samples exhibit similar grain sizes (except for $SrTiO_3$, where modified $SrTiO_3$ even show smaller grain size compared to pristine $SrTiO_3$), further confirming $LaNbO_4$ is not a sintering aid for the samples. Given the extremely thin dimension of their grain boundaries compared to those of LATP and NZSP (even smaller than the resolution limitation of SEM), atomic-resolution STEM was employed to study the grain boundaries.

Table 3. The mechanical properties of E_m and Σ_f for pristine and modified NZSP and LATP samples.

	NZSP pristine	NZSP modified	LATP pristine	LATP modified
Average elastic modulus E_m [GPa]	49	58	24	56
Standard deviation of E_m	7	15	2	11
Average fracture stress Σ_f [MPa]	79	88	37	77
Standard deviation of Σ_f	13	9	4	14

Figure 4 compares the microstructure of the grain boundaries of pristine and modified LLT, 8YSZ, and $SrTiO_3$. It should be emphasized that multiple and random positions were chosen in each sample to ensure a statistical significance. Figure 4 shows a typical example of each composition, while some additional examples are presented in Figure S9 (Supporting Information). In all three cases, the modified samples (right panel of Figure 4) show improved grain boundary contact, as evidenced by the atomically sharp connectivity between the lattice planes and the neighboring grains. The matter density at the grain boundaries is also significantly increased, particularly for modified 8YSZ and $SrTiO_3$ (Figure 4b,c), as indicated by the absence of a dark HAADF STEM contrast at grain boundaries of the pristine samples (left panel of Figure 4). This observation, in combination with the atomically sharp lattice contact, indicates that the grain boundaries of the modified samples merge almost perfectly with the adjacent grains, thus resulting in the improvement of grain boundary conductivity.

Moreover, elemental enrichment can be observed at the atomically contacted grain boundaries of modified LLT and 8YSZ, as shown in **Figure 5**. The enrichment of Nb is evident in the grain boundaries of modified LLT (Figure 5a), while the enrichment of La is observed in the grain boundaries of modified 8YSZ (Figure 5b). A reasonable doubt arises as to whether Nb or La alone reinforces the grain boundary of LLT or 8YSZ, respectively. It is challenging to distinguish only Nb or nominal $LaNbO_4$ as the tightener of the grain boundaries in LLT, especially since La itself is a major element in the ceramic. However, when La_2O_3 is added separately to pristine 8YSZ, a σ_{bulk} of 2.9×10^{-5} S cm^{-1} and a σ_{total} of 1.1×10^{-5} S cm^{-1} (both tested at 350 °C) are achieved (Figure S10, Supporting Information), with little difference to the values of pristine 8YSZ. This indicates that the reinforcement of the grain boundary of 8YSZ stems from the combined influence of La and Nb, rather than La alone, despite the fact that only La is observed in the grain boundary of modified 8YSZ. On the other hand, no clear enrichment is seen in the modified $SrTiO_3$ (Figure S11, Supporting Information), indicating that the additional elements are evenly distributed in the sample. This is reasonable because the solubility of La and Nb in $SrTiO_3$ is high.

In all samples of the five investigated ceramics, the distribution of elements in their grain boundaries appears irregular. In NZSP and LLZ, Nb enrichment is observed in the modified samples, while in 8YSZ, La enrichment is observed. However, in the cases of LATP and $SrTiO_3$, no enrichment of any element is observed. This ambiguity makes it difficult to determine how nominal $LaNbO_4$ affects the grain boundaries of these ceramics. One possible assumption is that a La-Nb-O related phase may appear in a certain sintering step of the investigated ceramics, thereby improving the microstructure of the grain boundaries, but it may not persist after sintering. Nonetheless, at this stage, it can be concluded that nominal $LaNbO_4$ (and not La or Nb alone) can effectively decrease the R_{gb} of NZSP, LATP, LLZ, 8YSZ, and $SrTiO_3$ ceramics by reinforcing the microstructure of their grain boundaries. However, the elucidation of a detailed mechanism still requires further investigation.

2.3. Discussions

The concept of R_{gb} in polycrystalline ceramics is generally well-understood and agreed upon in the literature. However, there is some debate regarding the definition of grain boundary conductivity (σ_{gb}). Some studies directly define σ_{gb} as:

$$\sigma_{gb} = \frac{l}{R_{gb}\, A} \tag{3}$$

where l is the thickness of the sample pellets, and A is the surface area. However, strictly speaking, this "σ_{gb}" should be considered an "apparent σ_{gb}," as it is based on the dimensions of the entire sample rather than the actual grain boundary. A true σ_{gb} needs to be calculated using the grain boundary's specific dimensions, which are typically a small fraction of the total sample dimensions. Only with a true σ_{gb} can the intrinsic conductivity of the grain boundary material (related to chemical circumstances like chemical composition, phases, defects etc. in the grain boundary, and independent of its geometry) be properly evaluated.

Determining the precise dimensions of grain boundaries in ceramics is challenging. To address this, a brick-layer model can be applied:[48]

$$\sigma_{gb} = \frac{l}{R_{gb}\, A} \frac{C_{bulk}}{C_{gb}} \tag{4}$$

where C_{bulk} and C_{gb} represent characteristic capacitance of the CPEs originating from the bulk and grain-boundary contribution (see Figure 1a and Table S2, Supporting Information), respectively. A "real σ_{gb}" as in Equation (4) can be easily calculated from the achieved data in the present work. Although σ_{gb} calculated this way is convenient, it assumes that the dielectric constants of the bulk and grain boundary are equal. This is highly debatable because they easily differ by orders of magnitude.[49–51] Nevertheless, the achieved σ_{gb} from Equation 4 is presented in Table S3 (Supporting Information).

With the above considerations, R_{gb} is mainly influenced by two factors: 1) Dimensional factor: This pertains to the microstructural geometry of the grain boundary, primarily the grain boundary thickness d. In pristine NZSP and LATP, poor grain-boundary

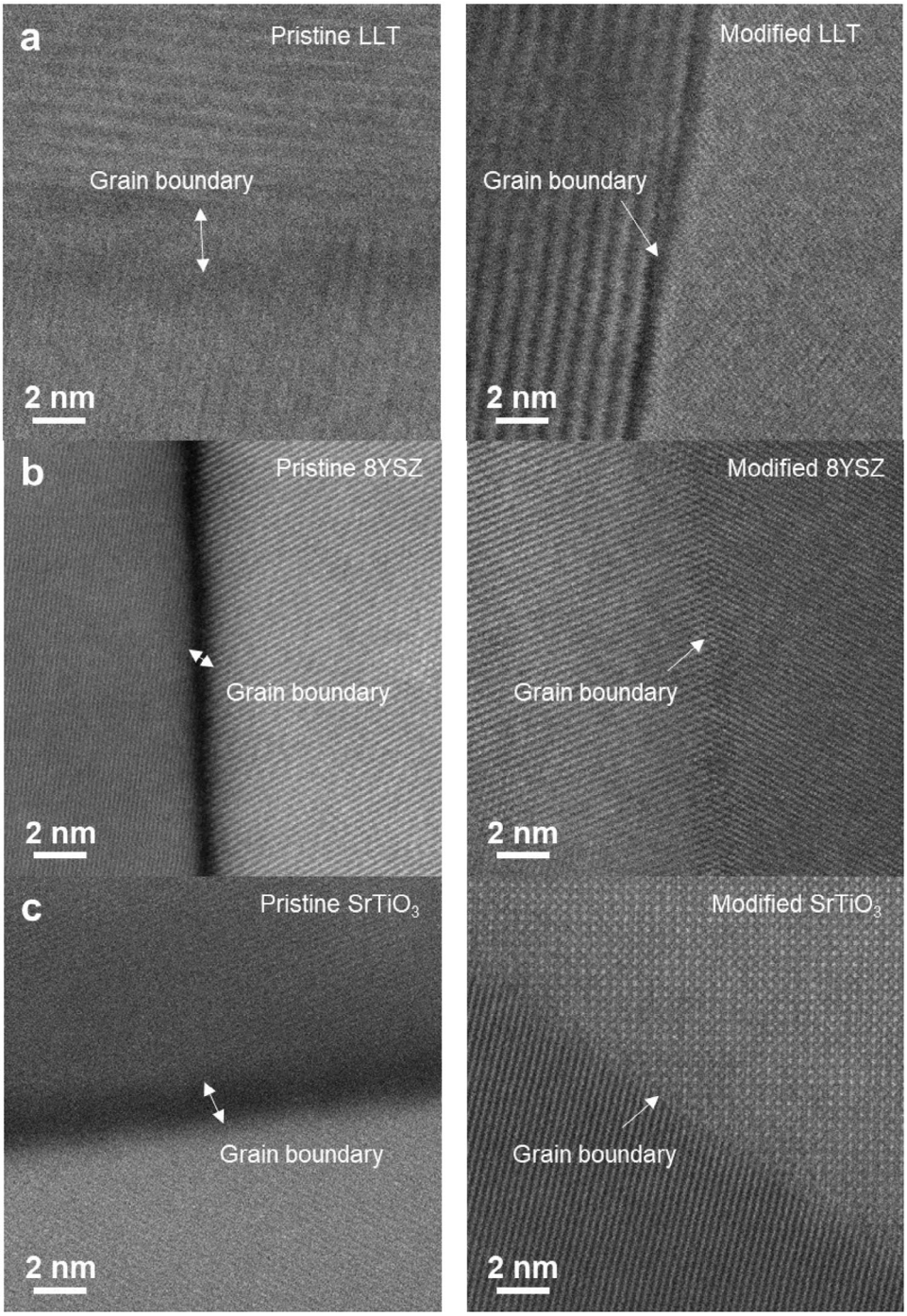

Figure 4. HAADF STEM investigations of a) pristine and modified LLT, b) pristine and modified 8YSZ, and c) pristine and modified $SrTiO_3$. The grain boundaries are tilted to an end-on configuration, while the lattice fringes of the neighboring grains are maintained.

reinforcement can result in an increased grain boundary thickness *d*, and even the formation of microcracks, as observed via SEM. These factors contribute to high R_{gb}. The thermal expansion anisotropy of both modified samples of NZSP and LATP, however, should not change significantly due to the following reasons: i) The addition of $LaNbO_4$ does not change the rhombohedral crystal structure. The pristine and modified samples show almost the same main phase (Figure S1, Supporting Information). ii) The σ_{bulk} values do not exhibit an essential difference between the pristine and modified samples. Therefore, the elimination of micro-cracks in the modified samples should not be directly correlated with thermal expansion anisotropy. Since for both materials, secondary phases are observed which fill the remaining pores at the triple grain junctions, it is reasonable to assume that they

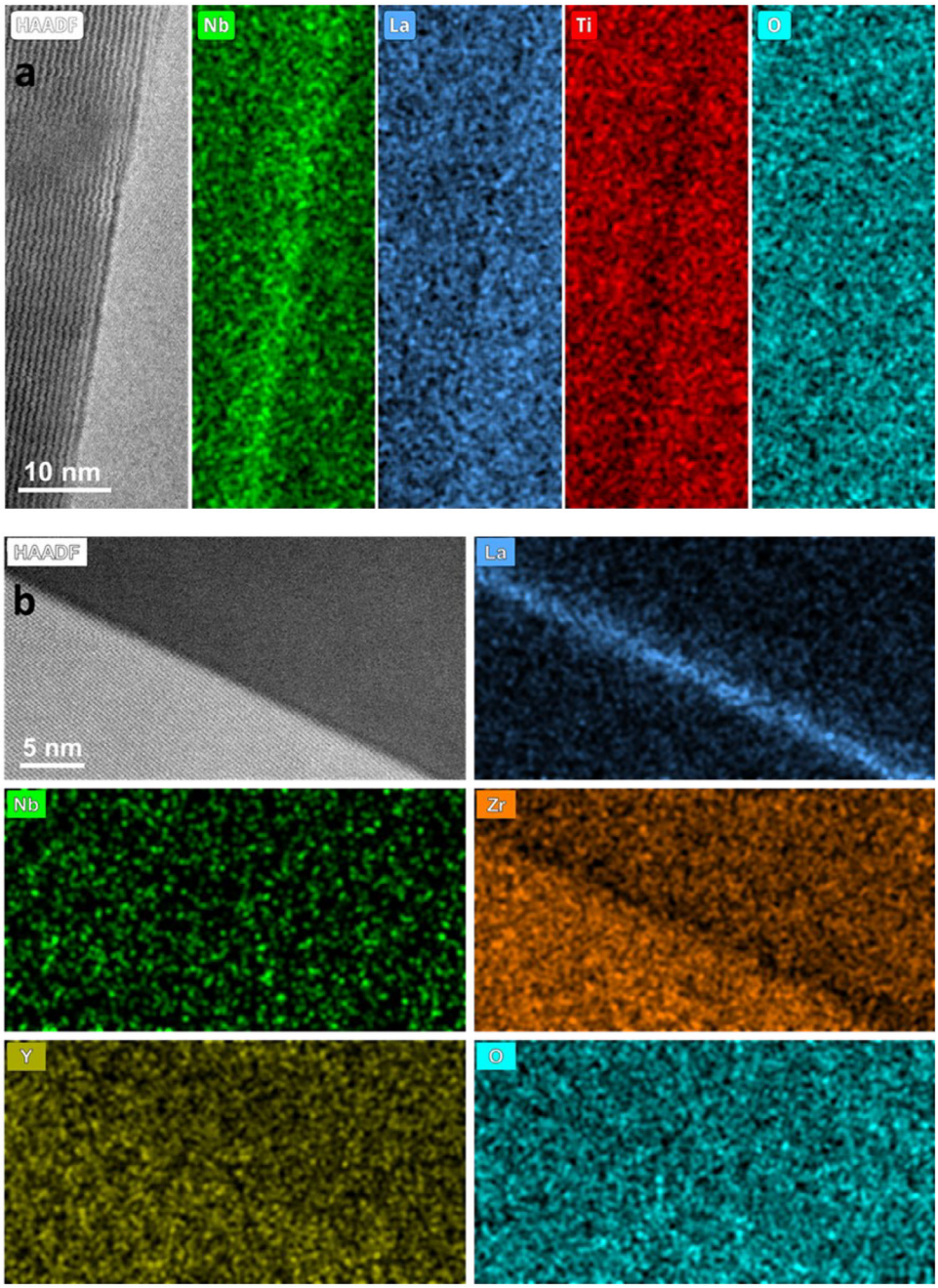

Figure 5. STEM investigations with EDS of modified a) LLT and b) 8YSZ.

can provide extra support for reinforcing the grain-to-grain contact. In particular, the crack-like boundaries seen in the modified NZSP sample can be mediated by Nb enrichment. For materials such as LLT, 8YSZ, and $SrTiO_3$, $LaNbO_4$ modification improves the grain-to-grain contact particularly at the atomic level, as observed by TEM. Since the element distribution of both La and Nb is almost all different for the different sintered ceramics, it is hard to determine the in-depth mechanism of how nominal $LaNbO_4$ reinforces the microstructure of the grain boundaries. In situ TEM observation is doubtless the best instrument to answer the question. However, because of the sensitive nature of NZSP and LATP under TEM beam (even at RT), and the too high sintering temperature of LLT, 8YSZ and $SrTiO_3$ (>1300 °C), more realistic considerations are still needed for the further investigations. 2) Chemical factor: The chemical composition, phases, and defects in the grain boundary also play significant roles. For the same reason of the complexity of grain-boundary compositions, phases and defects, it is difficult to discuss their contributions in general. Whereas for the investigation of the crystal chemistry of a ceramic, sufficient methods (like XRD, neutron scattering, nuclear magnetic resonance, X-ray photoelectron spectroscopy etc.) provide comprehensive data, the investigation of chemical

circumstances in the grain boundary can almost only rely on TEM. There are reports discussing the influence of chemical state related to R_{gb}. Space-charge layer models assume that depleted space-charge layers are the origin of the enhanced R_{gb}.[52] This model was also applied to explain the possible reason of extra high R_{gb} of LLT and $SrTiO_3$.[8,53] It should be noted that space-charge layers are influenced by geometry effects too.[54] With this consideration, the space-charge layers (if there is any) of all the discussed ceramics in the present work may be benefited from the decreased thickness d of the grain boundary with the modification of nominal $LaNbO_4$. It is also reported that La_2O_3 and/or Nb_2O_5 doped ceramics, especially perovskites, may exhibit high dielectric constants, effectively mitigating potential barriers at grain boundaries and decreasing R_{gb}.[49,51,55] However, these influences are only suitable to be analyzed on a case-by-case basis, not for a general consideration. A common observation for all the discussed ceramics is an increase in matter density within the grain boundaries. This is a proven finding that may lead to the decrease of R_{gb}. Further investigation is needed to confirm the underlying mechanism.

3. Conclusions

In summary, various well-known conductive ceramics such as NZSP, LATP, LLT, 8YSZ, and $SrTiO_3$ were prepared using solid-state reaction methods or sol–gel methods. For each material, both the pristine and 0.5-3 mol% $LaNbO_4$-modified ceramics were prepared using the same processes for better comparison. All the prepared ceramics within the same system exhibit a similar density (with a minimum of 93% of theoretical density), phase purity, and grain size. All pristine and modified samples of each material were exposed to the same sintering temperature and resulted in similar relative densities, indicating that $LaNbO_4$ is not a sintering aid for these ceramics. Although $LaNbO_4$-modified ceramics show similar or even lower σ_{bulk} compared to their pristine version at a fixed temperature, the σ_{total} value is always significantly higher. Separate addition of La or Nb does not show same effect. Notably, the σ_{total} values of modified NZSP and LATP are the highest among all published Na^+-ion- and Li^+-ion-conducting polycrystalline oxides (9.3×10^{-3} S cm^{-1} and 2.1×10^{-3} S cm^{-1} at 25 °C, respectively).

The improvement of the grain boundary microstructure, attributed to the addition of $LaNbO_4$, leads to lower R_{gb} and, consequently, higher σ_{total} in all these ceramics. Enhanced grain-to-grain contact and narrower and more crystalline grain boundaries with a higher matter density are determined in all the modified ceramics. These findings, which were observed for different ceramic systems with varying crystalline structures, charge carriers, and preparation methods, make $LaNbO_4$ an attractive option for improving the grain boundary resistance and grain boundary microstructure of other ceramics. However, the detailed mechanism by which $LaNbO_4$ influences the grain boundary microstructure requires further investigation.

4. Experimental Section

Materials: The powders were synthesized using either a solution-assisted solid-state reaction method (SASSR) for NZSP and LATP,[26] or by Pechini's method for the remaining compositions.[27] In the latter case, a double molar amount of citric acid and ethylene glycol with respect to the cations was added to the solutions of LLT, 8YSZ, and $SrTiO_3$. Since many preparation steps are similar for the five powders, the synthesis is described in detail and the different parameters can be taken from Figure S12 (Supporting Information). The chemicals used are listed in Table S4 (Supporting Information).

$NaNO_3$, $ZrO(NO_3)_2$, $Si(OCH_2CH_3)_4$, and $NH_4H_2PO_4$ were used as starting materials for the pristine NZSP powder. An additional 2 mol% of $LaNbO_4$ was applied for the modified NZSP with $NH4NbO(C_2O_4)_2$ and $La(NO_3)_3$ as starting materials. Stoichiometric amounts of $NaNO_3$ and $ZrO(NO_3)_2$ were dissolved in deionized water. For modified NZSP, $NH_4NbO(C_2O_4)_2$ and $La(NO_3)_3$ were also added in this step. A stoichiometric amount of $Si(OCH_2CH_3)_4$ was then added to the solution while stirring. When $Si(OCH_2CH_3)_4$ was hydrolyzed, the stoichiometric amount of $NH_4H_2PO_4$ was added to the system during stirring. The homogeneous aqueous solution immediately revealed the formation of complex zirconium oxyphosphate compounds. The whole mixture was dried at 85 °C. The dried powder was then calcined at 800 °C for 3 h. After calcination, a white powder was obtained. The calcined powder was then milled in ethanol with zirconia balls on a milling bench for 48 h, and dried at 70 °C for 12 h. The original and modified NZSP powders were put into a cylindrical pressing mold (8–13 mm in diameter) and pressed with a uniaxial pressure of about 100 MPa at room temperature. The pressed pellets were sintered between 1250 °C and 1300 °C for 5 h. The pellets obtained had a thickness of 1–2 mm.

LATP powders were prepared by the same method like that of NZSP. The differences are $LiNO_3$, $Al(NO_3)_3$ $9H_2O$, $Ti(OCH(CH_3)_2)_4$, $NH_4H_2PO_4$, $NH_4NbO(C_2O_4)_2$ and $La(NO_3)_3$ were applied as starting materials; The dried powder was calcined at 650 °C for 3 h; And the pressed pellets were sintered at 950 °C for 5 h.

Pristine LLT powders were prepared by Pechini's method. $Ti[OCH(CH_3)_2]_4$, $LiNO_3$ and $La(NO_3)_3$ were applied as the starting materials. Stoichiometric amounts of $LiNO_3$ and $La(NO_3)_3$ were dissolved in deionized water. Nitric acid was then added into the solution to keep the pH value of the solution at about 1. Stoichiometric amounts of $Ti[OCH(CH_3)_2]_4$ was slowly dissolved into the solution, followed by the double mole-amount of citric acid and ethylene glycol to the cations in the solution. The solution was evaporated and dried at a heating plate at 300 °C while stirring, then calcined at 800 °C. The calcined powder was then milled in ethanol with zirconia balls on a milling bench for 48 h, and dried at 70 °C. Modified LLT powder was prepared by adding 1 mol% La_2O_3 and Nb_2O_5 into the pristine LLT powders followed by ball-milling with zirconia balls on a milling bench for 72 h, and dried at 70 °C. The pristine and modified LLT powder was put into a cylindrical pressing mold (10–13 mm in diameter) and pressed with a uniaxial pressure of about 100 MPa at room temperature. The pressed pellets were sintered at 1325 °C for 5 h. The obtained pellets had a thickness of 1–2 mm.

The pristine and 0.5 mol% $LaNbO_4$-modified 8YSZ samples was added by Pechini's method. $ZrO(NO_3)_2$ and $Y(NO_3)_3$ were applied as the starting materials for pristine 8YSZ. 0.5 mol% of $LaNbO_4$ was added for modified 8YSZ with $NH_4NbO(C_2O_4)_2$ and $La(NO_3)_3$ as starting materials. Stoichiometric amounts of $ZrO(NO_3)_2$ and $Y(NO_3)_3$ were dissolved in deionized water. For modified 8YSZ, stoichiometric amounts of $NH_4NbO(C_2O_4)_2$ and $La(NO_3)_3$ were also added in this step. Double molar amount of citric acid and ethylene glycol to the cations were then added into the solution. The solution was evaporated and dried on a heating plate at 300 °C while stirring, then calcined at 900 °C. The calcined powder was then milled in ethanol with zirconia balls on a milling bench for 48 h, and dried at 70 °C. The pristine and modified 8YSZ powders were put into a cylindrical pressing mold (13–20 mm in diameter) and pressed with a uniaxial pressure of about 50 MPa at room temperature. The pressed pellets were sintered at 1400 °C for 5 h. The obtained pellets had a thickness of 1–2 mm.

The pristine and 1.0 mol% $LaNbO_4$-modified $SrTiO_3$ samples were synthesized using Pechini's method. $Sr(NO_3)_2$ and $Ti[OCH(CH_3)_2]_4$ were used as the starting materials. 1 mol% of $LaNbO_4$ was added for modified $SrTiO_3$ with $NH_4NbO(C_2O_4)_2$ and $La(NO_3)_3$ as starting materials.

Stoichiometric amount of $Sr(NO_3)_2$ was dissolved in deionized water. Nitric acid (65%, Aldrich) was then added into the solution to keep the pH value of the solution at about 1. For modified $SrTiO_3$, stoichiometric amount of $NH_4NbO(C_2O_4)_2$ and $La(NO_3)_3$ were also added in this step. Stoichiometric amount of $Ti[OCH(CH_3)_2]_4$ was slowly dissolved into the solution, followed by the double molar amount of citric acid and ethylene glycol to the cations in the solution. The solution was evaporated and dried on a heating plate at 300 °C while stirring, then calcined at 900 °C. The calcined powder was then milled in ethanol with zirconia balls on a milling bench for 48 h, and dried at 70 °C. The pristine and modified $SrTiO_3$ powders were put into a cylindrical pressing mold (8–13 mm in diameter) and pressed with a uniaxial pressure of about 100 MPa at room temperature. The pressed pellets were sintered at 1400 °C in 2% H_2-Ar for 5 h. The obtained pellets had a thickness of 1–2 mm.

Characterizations: The prepared dense pellets of pristine and modified NZSP, LATP, LLT, and $SrTiO_3$ were sputtered with gold on both sides. After sputtering, the edge of the samples was polished with sand paper to prevent the short-circuit caused by the residual Au on the edge. For 8YSZ, Ag paste was printed and sintered at 800 °C onto both sides of the pellets as the electrodes. The temperature-dependent impedance spectra of pristine and modified NZSP, LATP, LLT, and $SrTiO_3$ ranging from 100 °C to −100 °C were recorded with a commercial electrochemical system (Novocontrol Technologies Alpha-A) using a temperature-controlled chamber (Novocontrol Technologies BDS1100). For NZSP and LATP, extra impedance spectra of the samples were measured at 25 °C with two commercial electrochemical systems (Keysight E4991B and Novocontrol Technologies Alpha-A), with an AC frequency range of 3 GHz to 1 MHz and 10 MHz to 1 Hz, respectively. For 8YSZ, the temperature-dependent impedance spectra were investigated in the temperature range of 500 °C to 250 °C using a commercial electrochemical system (Novocontrol Technologies Alpha-A) including a temperature-controlling system and a furnace. The results were fitted using the "Z-view" software (Scribner Associates Inc.).

The microstructures of pristine and modified NZSP and LATP samples were analyzed using a Zeiss Merlin field-emission scanning electron microscope equipped with an EDS detector. The microstructure of the grain boundaries of all samples was investigated using high-angle annular dark-field scanning transmission electron microscopy (FEI Titan 80–200 ChemiSTEM), which is equipped with a Super-X EDS system, running at 200 kV. NZSP, LATP, and LLT samples for HAADF STEM were prepared using standard procedures including cutting, mechanical grinding, dimpling, and ion polishing under water-free conditions. The final thinning was carried out by means of 5 kV Ar-ion milling at liquid nitrogen temperature followed by a cleaning process at 1 kV (Gatan Precision Ion Polishing System II). 8YSZ and $SrTiO_3$ samples were prepared following a standard lift-out process using a focused ion beam (FIB) system (FEI Helios NanoLab 460F1). The thickness of the FIB sample was thinned below 100 nm to better investigate the images.

The ring-on-ring bending test is an often used to determine elastic modulus and fracture strength of ceramic materials. The experiments were performed using an electromechanical machine (INSTRON 1362) with a ±1000 N load cell (Lebow) and the displacement during the test was measured with the aid of a ceramic extension rod joined to a linear variable differential transformer (Solartron Metrology). The elastic modulus and maximum stress were obtained as outlined in ASTM C1499-05.[47] Tests were conducted at room temperature; the diameter of loading ring and supporting ring were 3.324 mm and 10.032 mm, respectively. More detailed descriptions of the procedures can be found in former references.[56,57] The average thickness and diameter of pristine and modified NZSP and LATP are at the range of 0.80–0.88 mm, 12.51–12.81 mm, respectively, and the number of tested specimens ranges from 6 to 18.

Supporting Information

Supporting Information is available from the Wiley Online Library or from the author.

Acknowledgements

L.L. and Y.L. contributed equally to this work. L.L. and X.Z. thank the National Key R&D Program of China (2021YFB4001502), the National Natural Science Foundation of China (No. 22075231), the Sichuan Science and Technology Program (No. 2021YFSY0022), and the Tianfu Yongxing Laboratory Organized Research Project Funding (No. 2023KJGG09) for financial support. X.L. thanks the China Scholarship Council Funding (No. 202308120016) for financial support.

Open access funding enabled and organized by Projekt DEAL.

Conflict of Interest

The authors declare no conflict of interest.

Data Availability Statement

The data that support the findings of this study are available from the corresponding author upon reasonable request.

Keywords

conductive ceramics, grain-boundary modification, grain-boundary resistance, lanthanum niobate

Received: October 26, 2024
Revised: December 12, 2024
Published online: January 2, 2025

[1] M. J. Verkerk, B. J. Middelhuis, A. J. Burggraaf, *Solid State Ionics* **1982**, *6*, 159.
[2] Q. Ma, C.-L. Tsai, X.-K. Wei, M. Heggen, F. Tietz, J. T. Irvine, *J. Mater. Chem. A* **2019**, *7*, 7766.
[3] S. D. Jackman, R. A. Cutler, *J. Power Sources* **2012**, *218*, 65.
[4] S. Breuer, D. Prutsch, Q. Ma, V. Epp, F. Preishuber-Pflügl, F. Tietz, M. Wilkening, *J. Mater. Chem. A* **2015**, *3*, 21343.
[5] Q. Ma, F. Tietz, *ChemElectroChem* **2020**, *7*, 2693.
[6] P. Mondal, A. Klein, W. Jaegermann, H. Hahn, *Solid State Ionics* **1999**, *118*, 331.
[7] C. Ma, K. Chen, C. Liang, C.-W. Nan, R. Ishikawa, K. More, M. Chi, *Energy Environ. Sci.* **2014**, *7*, 1638.
[8] J.-F. Wu, X. Guo, *Phys. Chem. Chem. Phys.* **2017**, *19*, 5880.
[9] W. J. Kwon, H. Kim, K.-N. Jung, W. Cho, S. H. Kim, J.-W. Lee, M.-S. Park, *J. Mater. Chem. A* **2017**, *5*, 6257.
[10] G. Hammerl, A. Schmehl, R. R. Schulz, B. Götz, H. Bielefeldt, C. W. Schneider, H. Hilgenkamp, J. Mannhart, *Nature* **2000**, *407*, 162.
[11] Z. Sun, E. Fabbri, L. Bi, E. Traversa, *Phys. Chem. Chem. Phys.* **2011**, *13*, 7692.
[12] H. Chung, B. Kang, *Solid State Ionics* **2014**, *263*, 125.
[13] J. H. Lee, T. Mori, J. G. Li, T. Ikegami, M. Komatsu, H. Haneda, *J. Electrochem. Soc.* **2000**, *147*, 2822.
[14] H. J. Avila-Paredes, K. Choi, C.-T. Chen, S. Kim, *J. Mater. Chem.* **2009**, *19*, 4837.
[15] S. Tiku, F. Kröger, *J. Am. Ceram. Soc.* **1980**, *63*, 183.
[16] C. A. Fisher, H. Matsubara, *J. Eur. Ceram. Soc.* **1999**, *19*, 703.
[17] T. Defferriere, D. Klotz, J. C. Gonzalez-Rosillo, J. L. Rupp, H. L. Tuller, *Nat. Mater.* **2022**, *21*, 438.
[18] S. Tsunekawa, H. Takei, *J. Phys. Soc. Jpn.* **1976**, *40*, 1523.
[19] L. Jian, R. D. James, *Acta Mater.* **1997**, *45*, 4271.
[20] L. Jian, C. Wayman, *Mater. Lett.* **1996**, *26*, 1.

[21] T. Takagi, Y. H. Choa, T. Sekino, K. Niihara, *Key Eng. Mater.* **1999**, *161*, 181.
[22] Z. Zhang, L. Zhou, Y. Hu, L. Jiang, *Scr. Mater.* **2002**, *47*, 637.
[23] W. He, Y. Ai, B. Liang, W. Chen, C. Liu, *Mater. Sci. Eng. A* **2018**, *723*, 134.
[24] B. Ma, B. Chi, J. Pu, L. Jian, *Int. J. Hydrogen Energy* **2013**, *38*, 4776.
[25] S. Maschio, G. Pezzotti, O. Sbaizero, *J. Eur. Ceram. Soc.* **1998**, *18*, 1779.
[26] Q. Ma, M. Guin, S. Naqash, C.-L. Tsai, F. Tietz, O. Guillon, *Chem. Mater.* **2016**, *28*, 4821.
[27] M. P. Pechini, US Patent No. 3330697, **1967**.
[28] J. T. Irvine, D. C. Sinclair, A. R. West, *Adv. Mater.* **1990**, *2*, 132.
[29] Q. Ma, F. Tietz, D. Stöver, *Solid State Ionics* **2011**, *192*, 535.
[30] N. F. Mott, *Rev. Mod. Phys.* **1968**, *40*, 677.
[31] Y. Liu, L. Liu, J. Peng, X. Zhou, D. Liang, L. Zhao, J. Su, B. Zhang, S. Li, N. Zhang, *J. Power Sources* **2022**, *518*, 230765.
[32] J. Briant, G. Farrington, *J. Solid State Chem.* **1980**, *33*, 385.
[33] W. S. Tang, K. Yoshida, A. V. Soloninin, R. V. Skoryunov, O. A. Babanova, A. V. Skripov, M. Dimitrievska, V. Stavila, S.-i. Orimo, T. J. Udovic, *ACS Energy Lett.* **2016**, *1*, 659.
[34] A. Hayashi, N. Masuzawa, S. Yubuchi, F. Tsuji, C. Hotehama, A. Sakuda, M. Tatsumisago, *Nat. Commun.* **2019**, *10*, 5266.
[35] Z. Zhang, Q. Zhang, J. Shi, Y. S. Chu, X. Yu, K. Xu, M. Ge, H. Yan, W. Li, L. Gu, *Adv. Energy Mater.* **2017**, *7*, 1601196.
[36] W. Xiao, J. Wang, L. Fan, J. Zhang, X. Li, *Energy Storage Mater.* **2019**, *19*, 379.
[37] Y. Kato, S. Hori, T. Saito, K. Suzuki, M. Hirayama, A. Mitsui, M. Yonemura, H. Iba, R. Kanno, *Nat. Energy* **2016**, *1*, 16030.
[38] C. Wang, K. Fu, S. P. Kammampata, D. W. McOwen, A. J. Samson, L. Zhang, G. T. Hitz, A. M. Nolan, E. D. Wachsman, Y. Mo, *Chem. Rev.* **2020**, *120*, 4257.
[39] C.-L. Tsai, S. Yu, H. Tempel, H. Kungl, R.-A. Eichel, *Mater. Technol.* **2020**, *35*, 656.
[40] Y. Sun, P. Guan, Y. Liu, H. Xu, S. Li, D. Chu, *Crit. Rev. Solid State Mater. Sci.* **2019**, *44*, 265.
[41] K. Chen, M. Huang, Y. Shen, Y. Lin, C. Nan, *Solid State Ionics* **2013**, *235*, 8.
[42] J. Zhang, X. Huang, H. Zhang, Q. Xue, H. Xu, L. Wang, Z. Feng, *RSC Adv.* **2017**, *7*, 39153.
[43] X. Guo, J. Fleig, J. Maier, *J. Electrochem. Soc.* **2001**, *148*, J50.
[44] B. Odekirk, U. Balachandran, N. G. Eror, J. Blakemore, *J. Am. Ceram. Soc.* **1983**, *66*, C22.
[45] W. Gong, H. Yun, Y. Ning, J. Greedan, W. Datars, C. Stager, *J. Solid State Chem.* **1991**, *90*, 320.
[46] Z. Ding, Y. Tang, V. S. K. Chakravadhanula, Q. Ma, F. Tietz, Y. Dai, T. Scherer, C. Kübel, *Microscopy* **2023**, *72*, 326.
[47] *Standard Test Method for Monotonic Equibiaxial Flexural Strength of Advanced Ceramics at Ambient Temperature*, Standard ASTM, West Conshohocken, **2005**, pp. C1499-05.
[48] S. Haile, G. Staneff, K. Ryu, *J. Mater. Sci.* **2001**, *36*, 1149.
[49] S. Upadhyay, D. Kumar, O. Parkash, *Bull. Mater. Sci.* **1996**, *19*, 513.
[50] K. M. Batoo, S. Kumar, C. G. Lee, *Curr. Appl. Phys.* **2009**, *9*, 1397.
[51] A. Thomas, M. George, D. Sajan, K. Abraham, J. Thomas, K. Saban, *Opt. Mater.* **2019**, *89*, 299.
[52] J. Maier, *Angew. Chem., Int. Ed.* **1993**, *32*, 313.
[53] S. Rodewald, J. Fleig, J. Maier, *J. Am. Ceram. Soc.* **2001**, *84*, 521.
[54] I. Lubomirsky, J. Fleig, J. Maier, *J. Appl. Phys.* **2002**, *92*, 6819.
[55] X. Wang, Y. Zheng, B. Liang, G. Zhang, Y. Shi, B. Zhang, L. Xue, S. Shang, J. Shang, S. Yin, *J. Mater. Sci.: Mater. Electron.* **2020**, *31*, 16044.
[56] J. Malzbender, R. Steinbrech, *Surf. Coat. Technol.* **2004**, *176*, 165.
[57] J. Malzbender, R. W. Steinbrech, L. Singheiser, *Ceram. Eng. Sci. Proc.* **2005**, *26*, 293.